Journal of Nuclear Materials 377 (2008) 201–205

Contents lists available at ScienceDirect

Journal of Nuclear Materials

journal homepage: www.elsevier.com/locate/jnucmat

Nano-indentation measurement of oxide layers formed in LBE on F/M steels

P. Hosemann [a,b,*], J.G. Swadener [a], J. Welch [c], N. Li [a]

[a] Los Alamos National Laboratory, P.O. Box 1663, Los Alamos, NM 87545, USA
[b] Montanuniversität Leoben, Franz-Josef Strasse 18, 8700 Leoben, Austria
[c] University of Nevada Las Vegas, 4505 S. Maryland Parkway, Las Vegas, Nevada 89154-4001 USA

A B S T R A C T

Ferritic/martensitic (F/M) steels (T91, HT-9, EP 823) are candidate materials for future liquid lead or lead bismuth eutectic (LBE) cooled nuclear reactors. To understand the corrosion of these materials in LBE, samples of each material were exposed at 535 °C for 600 h and 200 h at an oxygen content of 10^{-6} wt%. After the corrosion tests, the samples were analyzed using SEM, WDX and nano-indentation in cross section. Multi-layered oxide scales were found on the sample surfaces. The compositions of these oxide layers are not entirely in agreement with the literature. The nano-indentation results showed that the E-modulus and hardness of the oxide layers are significantly lower than the values for dense bulk oxide materials. It is assumed that the low values stem from high porosity in the oxide layers. Comparison with in-air oxidized steels show that the E-modulus decreases with increasing oxide layer thickness.

1. Introduction

Ferritic/martensitic (F/M) steels (HT-9, T91, EP823) are candidate materials for advanced fast reactors and accelerator driven systems [1–3]. Liquid lead bismuth eutectic (LBE) is a candidate coolant for these applications. To study the corrosion resistance of the candidate materials they are being widely tested in flowing LBE. Since many of the steel alloying elements have a high solubility in LBE [1,2] some passivation mechanism on steel surfaces has to be used for protection. One strategy is to control the oxygen content of the LBE at a level of approximately 10^{-6} wt% using either gas phase or solid phase oxygen control systems [4–6]. This allows the formation of a 'self-healing' oxide layer on the steel surfaces and protects the materials underneath from dissolution. This protective oxide layer has to be dense and needs to stay on the surface as long as possible without forming cracks or pores through which LBE can contact the substrate steels. In order to ensure good long-term performance, the oxide growth mechanism and kinetics, the oxide layer structure and the oxide–steel interface bonding has to be thoroughly investigated. In this study, a 200 h and 600 h corrosion experiment was conducted in the DELTA Loop at Los Alamos National Laboratory (LANL). These relativly short exposure times allow studying the initial corrosion phenomena and to make estimations for the long-term exposure. The corrosion experiment is followed by nano-indentation, composition measurements and microscopy measurements on these oxide layers. This detailed analysis is to understand better the oxide layer structure as well as their mechanical integrity as a corrosion barrier.

2. Experiment

The materials shown in Table 1 were exposed to flowing (2 m/s in the sample test section) LBE for 200 h and 600 h at 535 °C in the DELTA Loop at LANL. The oxygen content in the LBE was controlled to be in the range of 10^{-6} wt% and the oxygen sensors were YSZ (yttria stabilized zirconia) membrane sensors with bismuth oxide reference electrodes. After exposure to LBE, the samples were cut and cross section samples prepared. The last polishing step uses 1/10 μm diamond polishing paste. The 600 h samples were analyzed using a Nano-indenter II instrument. The nano-indention measurements were performed using a Berkovic indenter. An indentation matrix of 4 rows and 10 columns was set. These 10 indents are always in the same distance from the sample surface. This leads to a total of 40 indents per sample which will provide sufficient data with good statistics. Each indent is 4 μm away from its surrounding indents. After performing these indentation measurements all the samples (200 h and 600 h) are analyzed using scanning electron microscope (SEM). Wavelength dispersion X-ray (WDX) analysis is performed only on the 600 h samples. The SEM analysis uses a JEOL JMS-5600 instrument. The WDX measurements were performed with a WDX detector on a JXA-8900 Super Probe microscope. Using the SEM micrographs each nano-indent on the 600 h samples is assigned to corresponding areas of epoxy, outer layer, inner layer or bulk steel. If a clear assignment is not possible because the indent is located too close to the interface

* Corresponding author. Address: Los Alamos National Laboratory, USA.
E-mail address: peterh@lanl.gov (P. Hosemann).

0022-3115/$ - see front matter © 2008 Elsevier B.V. All rights reserved.
doi:10.1016/j.jnucmat.2008.02.073

Table 1
Compositions of steels tested in LBE for 200 and 600 h at 535 °C

Material	Fe	Cr	Mo	Si	C	Mn
T91	Balance	9.3	0.95	0.43	0.1	–
HT-9	Balance	11.95	1.0	0.4	0.2	0.6
EP823	Balance	12	0.9	1.3	0.18	0.8

Table 2
Oxide thickness on each samples measured in SEM

Material	Oxide layer thickness (μm)		Remarks
	200 h	600 h	
HT-9	8–10	10–14	Double layer
T91	0–5	10–12	Double layer
EP823	4–6	6–11	Outer layer and partial inner layer

between to neighboring areas, the data is placed in between these two areas in the diagrams showing the results.

3. Results

The results of the oxide layer thickness measurements using SEM are shown in Table 2. The oxidation rate decreases with increasing exposure time of all the tested samples, as expected. The results of each tested material are described in detail below.

3.1. T91

The WDX and nano-indentation results are shown in Fig. 1. The SEM image shows a two-layer structure on the surface. The outer layer has a denser appearance than the inner layer. The cross sectional surface of the inner layer appears rougher. The nano-indents are visible in this image. The WDX measurements show a silicon enrichment at the interface between these two layers and a slight chromium enrichment throughout both layers. The iron and the oxygen show a step-like distribution in the layers (see Fig. 1). Most interestingly, the hardness throughout the layers does not increase significantly and the E-modulus drops in the inner layer more than 50% relative to the steel and increases slightly in the outer layer.

3.2. HT-9

This material behaves very similarly to T91 in the tests. The sample clearly (see Fig. 2) shows a double oxide layer structure in the SEM image. It appears that the outer layer is denser than the inner layer. The nano-indents can be seen in the SEM image. The WDX line scan also appears to be very similar to T91 although the Cr concentration is higher throughout the oxide layer. This cor-

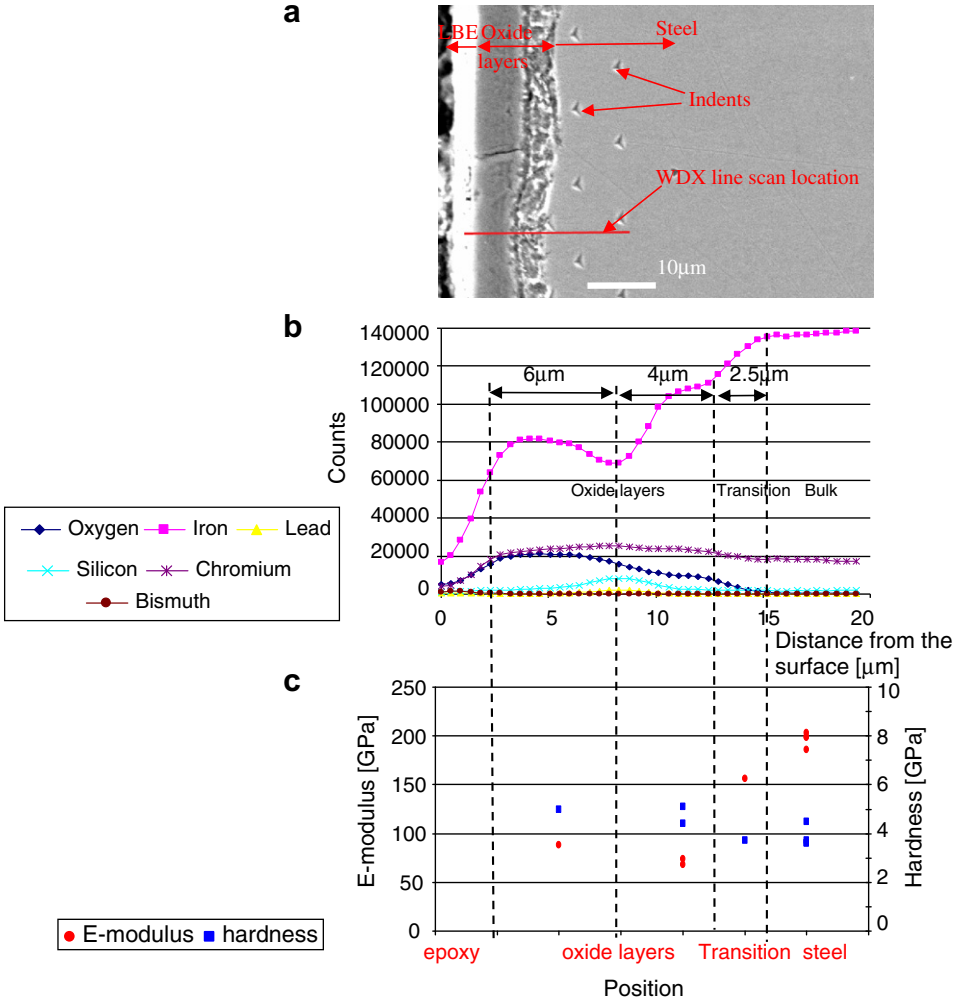

Fig. 1. SEM (a), WDX (b) and nano-indentation (c) results of the material T91. Each data point in the nano-indentation graph represents an average of 10 indents. The maximum standard deviation of the hardness values is 1.1 GPa and the maximum standard deviation of the E-modulus values is 29 GPa.

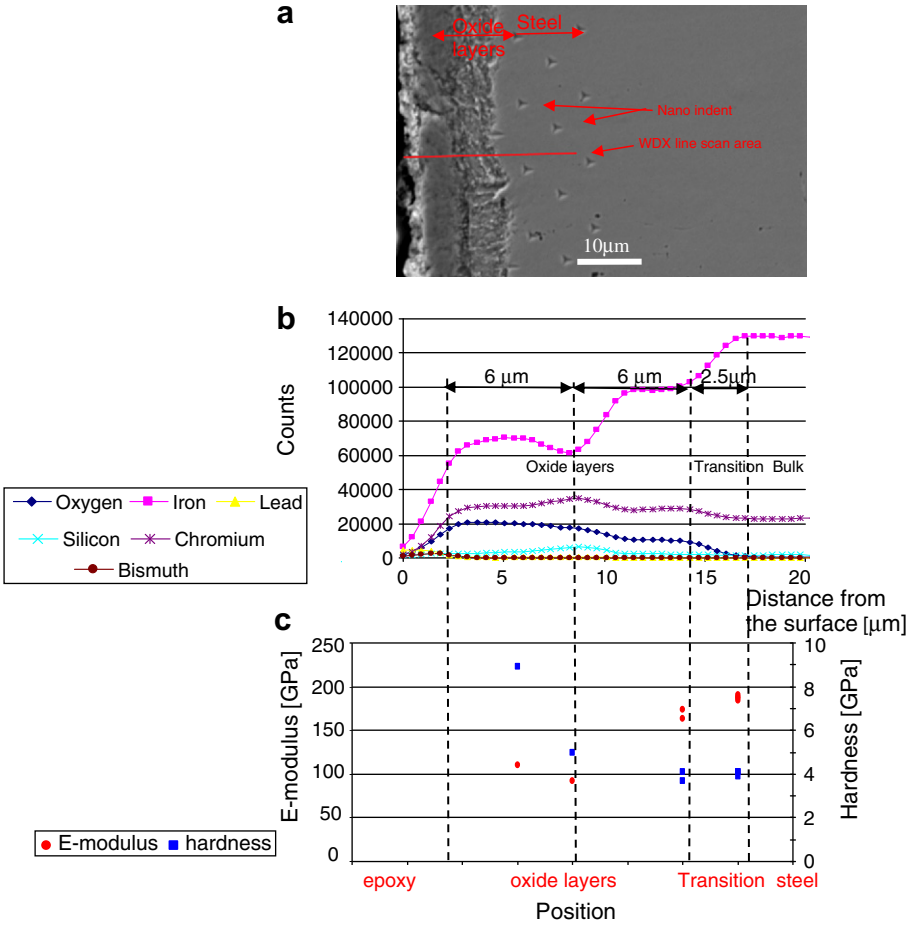

Fig. 2. (a) SEM image, (b) WDX and (c) nano-indentation test results of HT-9. Each data point in the nano-indentation graph represents an average of 10 indents. The standard deviation of the hardness values is 0.9 GPa and the standard deviation of the E-modulus values is 20 GPa.

responds to the higher Cr content in the bulk material. A difference can be seen in the nano-indentation results. A significant increase in the hardness is observed in the outer layer up to 9 GPa. But the E-modulus shows only a slight increase in comparison to T91.

3.3. EP823

The SEM image in Fig. 3 shows a dense outer layer and a partial inner layer. The inner layer was found to be discontinuous in the cross section. The WDX line scan was performed in a double layered area. Silicon enrichment was found throughout both layers and was slightly higher in the outer layer. The chromium enrichment throughout both layers seems to be very homogeneous, similar to the observations on the HT-9 oxide layer while the iron and oxygen show step-like distributions. The nano-indentation in the inner layer showed inconclusive results because the inner layer was discontinuous. Therefore the indents were mainly placed in the area of the inner layer-bulk transition and could not be assigned to the corresponding area as clearly as for HT-9 or T91. A large increase in hardness was observed in the outer layer, similar to that observed for HT-9, while the E-modulus drops in the outer layer relative to the bulk hardness (Fig. 4).

4. Discussion

The oxide layers of all three alloys in SEM analysis appear similar to what is documented in the literature [7–9]. A multiple oxide layer structure was found. But the WDX measurements revealed differences to what was reported in the literature [8,9]. The measurements performed here do not show a clear outer Fe_3O_4 layer and an inner $(Fe, Cr)_2O_3$ layer. In this study Cr was found throughout both oxide layers. It seems that the Fe_3O_4 layer either did not form in the beginning or was simply removed from the surface by the LBE flow. The difference between the inner layer and outer layer found here seem to be in the structure (appearance) and different levels of Cr, O, Fe or Si. To this point it is not clear what caused this segregation of alloying elements in both layers. In all the analyzed samples some silicon enrichment is found at the interface between the inner and outer layers. EP823, which showed the thinnest oxide layers, had significant silicon enrichment in both oxide layers. This is a confirmation that silicon enrichment leads to enhanced corrosion resistance, as is evidenced by the thinner oxide layer observed in EP823 when compared to that of HT-9 and T91.

The nano-indentation testing showed that the hardness only increases slightly in the oxide layer. This is somewhat unexpected because the hardness of oxides formed on Fe–Cr alloys is reported in the literature to be 18–33 GPa [14] and 18–37 GPa on pure Cr_2O_3 [13]. The nano-indentation size effect [10–12] would lead us to expect a higher hardness reading for the nano-indentation than the reported hardness data from the literature but quite the opposite was found. The E-modulus results gained from the same measurements show that the E-modulus in the oxide layers is more than 50% lower than in the bulk steels. This is also in contrast to bulk E-modulus data in the literature, which is reported to be 280–296 GPa [14] for a dense Fe–Cr oxide formed on steel and

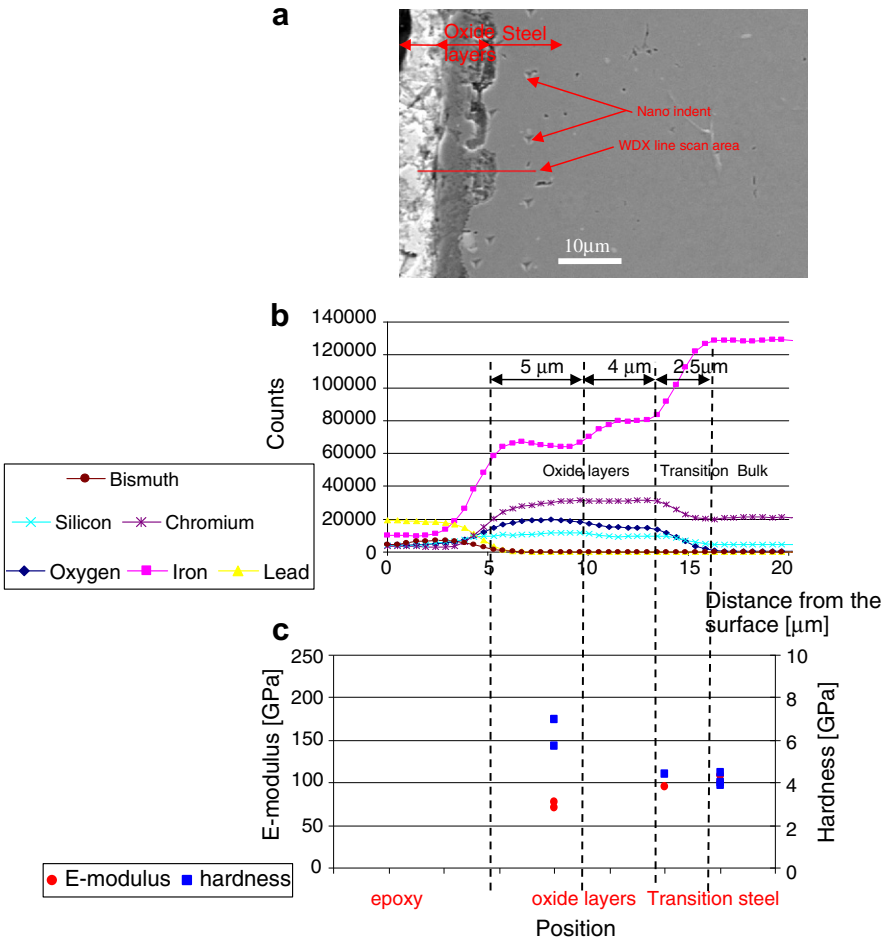

Fig. 3. (a) SEM image, (b) WDX and (c) nano-indentation test results of EP823. Each data point in the nano-indentation graph represents an average of 10 indents. The maximum standard deviation of the hardness values is 1 GPa and the maximum standard deviation of the E-modulus values is 15 GPa.

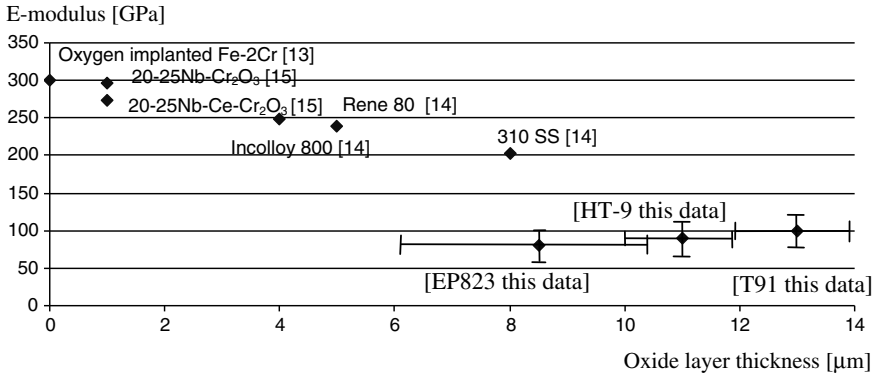

Fig. 4. Measure E-modulus compared with those reported in the literature [13–15].

273–300 GPa [13] for Cr_2O_3. These values are more than 3 times higher than the values measured here. Since the E-modulus of a material should remain constant as long as the composition and structure is the same the likely explanation of the different results is that the oxide layers grown in this experiment are highly porous and not dense as the implanted or sintered materials reported in the literature. Nicholls et al. proposes that oxides grown on various steels become more porous as they grow thicker [14]. It is assumed (as proposed by Nicholls et al. [14]) that the porosity of the oxide increases with increasing oxide layer thickness which causes a E-modulus or hardness reading lower than reported previously in the literature for dense oxide of similar composition. In addition to this general relation between oxide layer thickness and E-modulus the nano-indentation tests also showed that the inner oxide layer is softer than the outer oxide layer. This might be due to the fact that the inner oxide layer has higher porosity than the outer layer. The appearance of the oxide layers in the SEM cross section confirms this assumption.

In this study it was not evaluated if there is a difference between nano-indents placed on a grain boundary or not. The values here are average values over 10 indents.

5. Conclusions

- The LBE corrosion experiment in the DELTA Loop on T91 HT-9 and EP823 conducted for 600 h at 535 °C showed multi-layer oxides on the tested materials. Two different oxide layers were identified with different mechanical properties and different chemical composition.
- The WDX measurements on the cross sections revealed two Cr and Fe containing oxide layers and no Fe_3O_4 layer. It appears that the main difference between observed oxide layers is the Fe content and the micro-structure.
- All alloys showed silicon enrichment in the interface between the inner and outer oxide layers.
- Nano-indentation tests across the oxide layers were performed and showed low values of E-modulus in these oxide layers than the bulk steel and the E-modulus reported in the literature. Lower hardness values of the oxides than fully dense Fe–Cr oxides were also found.
- It seems that the lower E-modulus and hardness readings of the oxides are due to the increasing amount of pores in the oxide layers.

Acknowledgements

The authors wish to thank Professor Gregor Mori (Institute of Chemistry at the University of Leoben, Austria) for fruitful scientific discussions. Michael Madrid (Los Alamos National Laboratory, USA) for his support of the DELTA Loop operation. And Professor Allen Johnson (University of Nevada Las Vegas, USA) for supporting the SEM and EDX work.

References

[1] S.A. Maloy, T. Romero, M.R. James, Y. Dai, J. Nucl. Mater. 356 (2006) 56.
[2] J. Van den Bosch, D. Sapundjiev, A. Almazouzi, J. Nucl. Mater. 356 (2006) 237.
[3] Y. Kurata, M. Futakawa, S. Saito, J. Nucl. Mater. 343 (2005) 333.
[4] N. Li, J. Nucl. Mater. 300 (2002) 73.
[5] J. Weeks, A.J. Romano, Corrosion 25 (3) (1969) 131.
[6] Handbook on Lead–Bismuth Eutectic Alloy and Lead Properties, Materials Compatibility, Thermal-hydraulics and Technologies, 2007 Edition, ISBN 978-92-64-99002-9.
[7] J. Zhang, N. Li, Y. Chen, A.E. Rusanov, J. Nucl. Mater. 336 (2005) 1.
[8] F. Barbier, A. Rusanov, J. Nucl. Mater. 296 (2001) 231.
[9] H. Glasbrenner, J. Konys, G. Mueller, A. Rusanov, J. Nucl. Mater. 296 (2001) 237.
[10] W.D. Nix, H. Gao, J. Mech. Phys. Solids 46 (1998) 411.
[11] J.G. Swadener, E.P. George, G.M. Pharr, J. Mech. Phys. Solids 50 (2002) 681.
[12] F. Schulz, H. Hanemann, Z. Metallkd. 33 (3) (1941) 124.
[13] P.F. Tortorelli, J. Phys. IV 3 (1993) 943.
[14] J.R. Nicholls, D.J. Hall, P.F. Tortorelli, Mater. High Temp. 12 (1994) 141.
[15] P.F. Tortorelli, J.P. Keiser, K.R. Wilson, W.C. Oliver, Microscopy of Oxidation, The Institute of Metals, London, 1991. p. 271.